

# Studying That Smile

A tutorial on multispectral imaging of paintings using the *Mona Lisa* as a case study

**D**igital image capture to faithfully record fine art paintings is a fundamental task in a cultural heritage domain which is increasingly benefiting from the possibilities afforded by computer systems and art databases. Indeed, the digital format greatly facilitates in the archiving, retrieval, and dissemination of art [1]. Many museums, archives, and libraries have for some years been engaged in direct digital image capture of cultural heritage [2]. Digital imaging also opens the door to new postprocessing applications for conservation or restoration, such as art digital diagnosis and virtual restoration of paintings [3]. In this context, multispectral imaging has taken a prominent role—in the first instance, for generating high-fidelity color reproductions and, second, for their use as image spectrometers giving the spectral signature of each image element of the painting. This article offers a tutorial description of multispectral systems exemplified by the multispectral capture of the *Mona Lisa* by Leonardo da Vinci. This acquisition was performed at the Louvre Museum in Paris, France, in October 2004 and was an important achievement of the conservation restoration innovation systems for image capture and digital archiving to enhance training, education, and lifelong learning (CRISATEL) European Union project. This project was the latest in a series of pioneering projects on the digital acquisition of paintings which started with the visual art system for archiving and retrieval of images (VASARI) project in 1989 [4]. Examples of similar or related projects can be found in Europe [5], the United States [6], and Japan [7]. Another introduction to the imaging of fine art paintings can be found in [8].

A description of multispectral image capture is presented from a signal processing point of view. Indeed, this article is based on an equation that models the multispectral



© 1995 MASTER SERIES

## Analysis of Visual Cultural Heritage

acquisition of images. The main components of this equation are described. They correspond to the lighting conditions, the filters, the sensor sensitivity, and associated noise sources. Moreover, the optimization problems involved in the design of multispectral cameras, their calibration, and the processing of the obtained data are introduced within the same mathematical framework.

### THE ACQUISITION MODEL

The main components involved in an image acquisition process are depicted in Figure 1. We denote the spectral radiance of the illuminant by  $I(\lambda)$ , the spectral reflectance of the object surface imaged in a pixel by  $r(\lambda)$ , the spectral transmittance of the  $k$ th optical color filter by  $f_k(\lambda)$  and the spectral sensitivity of the sensor array by  $\alpha(\lambda)$ . Supposing a linear optoelectronic transfer function of the acquisition system, the camera response  $c_k$  for an image pixel is then equal to

$$c_k = \int_{\Lambda} I(\lambda) r(\lambda) f_k(\lambda) \alpha(\lambda) d\lambda + n_k, \quad (1)$$

where  $n_k$  is an additive noise and  $\Lambda$  is the range of the spectrum where the camera is sensitive. Only one optical color filter is represented in Figure 1, but in a multispectral capture system  $K$  images are acquired. A set of filters is often set up in a barrel, which rotates to automatically change filters between acquisitions. There also exist systems that do not need any mechanical displacement in order to change the filter transmittance. For instance, liquid crystal tunable filters (LCTFs) provide this capability. They are basically an accumulation of different layers, each layer containing linear parallel polarizers sandwiching a liquid crystal retarder element. See [9] and [10] for examples of its use and [11] for a short tutorial.

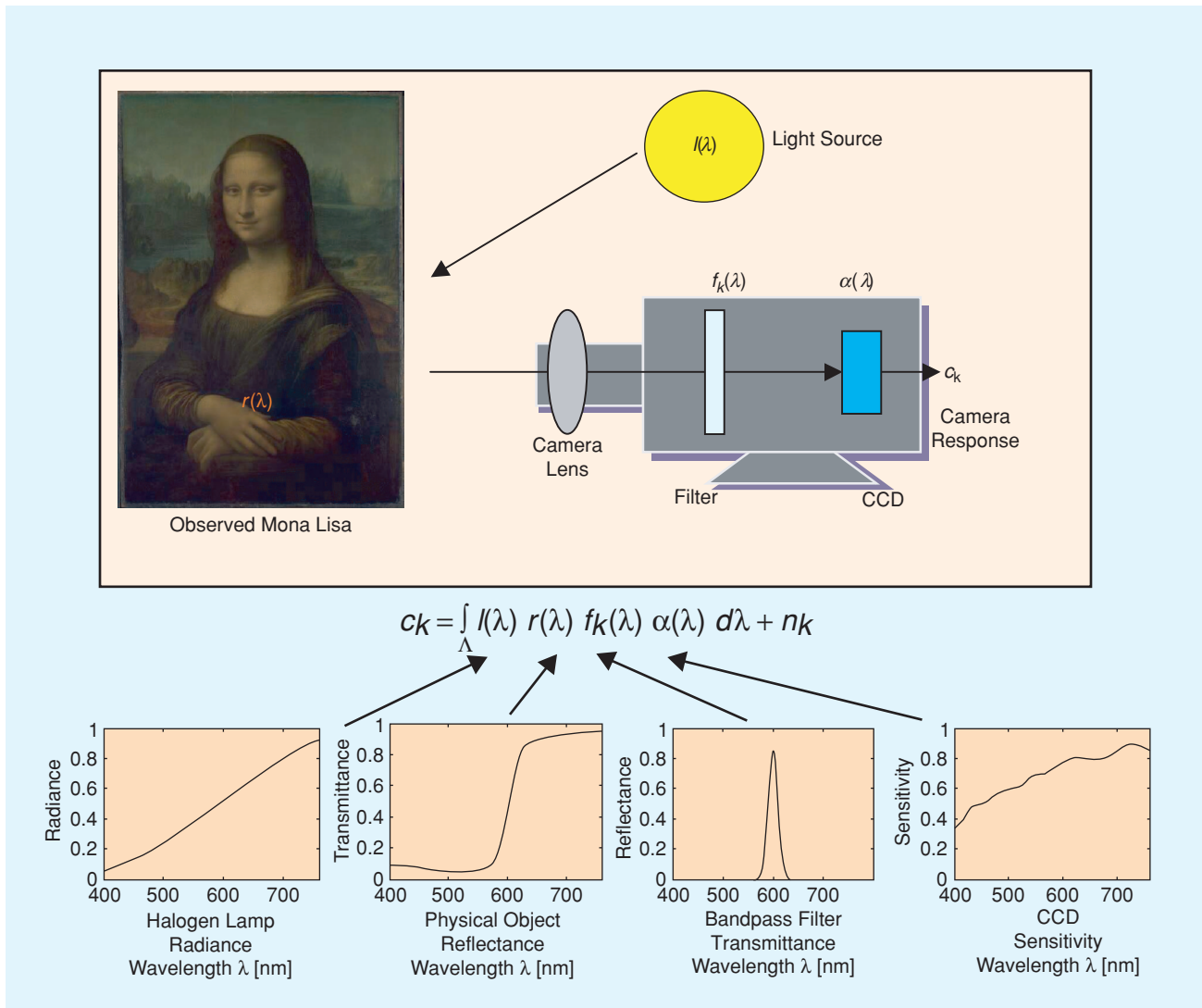


**[FIG1]** Schematic view of the image acquisition process. The camera response depends on the spectral radiance of the light source, the spectral reflectance of the objects in the scene, the spectral transmittance of the color filter, and the spectral sensitivity of the sensor. (*Mona Lisa* courtesy of the Centre de Recherche et de Restauration des Musées de France.)

For the digital capture of fine art paintings, the number of  $K$  filters ranges from  $K = 7$  [4] to recent  $K = 32$  [12], depending on the size of the filter band. The system described in this article uses 13 filters. For reference, commercial color digital cameras contain  $K = 3$  filters. For paintings, it is also common to use multispectral cameras as image spectrometers that aim to recover  $r(\lambda)$  at every image element of the artwork. In this case, (1) can be rewritten as

$$c_k = \int_{\Lambda} \phi_k(\lambda) r(\lambda) d\lambda + n_k, \quad (2)$$

where  $\phi_k(\lambda) = l(\lambda) f_k(\lambda) \alpha(\lambda)$  denotes the combined illuminant and the spectral sensitivity ( $f_k(\lambda)\alpha(\lambda)$ ) of the  $k$ th channel, which we call the augmented spectral sensitivity.

### SPECTRAL REFLECTANCE AND COLOR

The color of a surface point lit by a given illuminant can be easily predicted when the spectral reflectance of the surface at that point and the relative spectral power distribution of the illuminant are known. This color can be represented by just a triplet of numbers, the tristimulus values. This is due to the color vision trivariance property of a human observer and the presence in the retina of three types of cone photoreceptors. Furthermore, psychophysical experiments dating from the 1920s have shown that any color can be matched by a human observer with a mixture of three fixed primaries whose radiant powers have been suitably adjusted. The tristimulus values represent, therefore, the relative amount of energy of the primaries when the match is obtained. To fully define a colorimetric system, three primaries and a white reference must be chosen. The tristimulus values of the reference white are by definition all equal to one. The color matching experiments follow linear properties (Grassmann's law [13]). From these laws, if we sam-

ple the visible spectrum with a set of monochromatic wavelengths of the same energy and measure the tristimulus values for each of them, we obtain the color matching functions of the human observer for the chosen colorimetric system. With these functions we can then directly deduce the tristimulus values of any color from a colorimetric formula if we know its spectral power distribution. To avoid the selection of an arbitrary set of physical primaries, the Commission Internationale de l'Eclairage (CIE) has chosen a set of standard virtual primaries and has defined the CIE 1931 XYZ Standard Colorimetric Observer. The corresponding color matching functions are designated  $\bar{x}(\lambda)$ ,  $\bar{y}(\lambda)$ , and  $\bar{z}(\lambda)$ , and are positively valued (see Figure 2). The  $X$ ,  $Y$ , and  $Z$  tristimulus values of a surface point are calculated by integrating the product of its spectral reflectance  $r(\lambda)$ , the illuminant power distribution  $l(\lambda)$ , and the corresponding color matching function as follows:

$$X = \int_{\lambda_{\min}}^{\lambda_{\max}} r(\lambda) l(\lambda) \bar{x}(\lambda) d\lambda, \quad Y = \int_{\lambda_{\min}}^{\lambda_{\max}} r(\lambda) l(\lambda) \bar{y}(\lambda) d\lambda, \\ Z = \int_{\lambda_{\min}}^{\lambda_{\max}} r(\lambda) l(\lambda) \bar{z}(\lambda) d\lambda, \quad (3)$$

where usually  $\lambda_{\min} = 380$  and  $\lambda_{\max} = 760$  nm. From the above equations, it is simple to understand the relationship between spectral reflectance and color. These three equations can be seen as a simplification of (1) where the three color matching functions take the place of the camera functions product  $f_k(\lambda) \alpha(\lambda)$ . We note that the lighting conditions can be easily simulated, allowing us to perform "illuminant simulation" by just changing  $l(\lambda)$  to another light power distribution.

Due to its virtual primaries, the CIE 1931 XYZ color space is device independent. XYZ tristimulus values can be converted into a device-dependent color space, such as RGB for monitors or CMYK for printers via a color profile [14], or alternatively into a psychometric color space such as CIE 1976  $L^*a^*b^*$  (CIELAB). CIELAB is a widely used color space for accurate colorimetric analysis, both within industry and the scientific domain. It is a three-dimensional (3-D) space where the axes  $L^*$ ,  $a^*$ , and  $b^*$  represent lightness, redness/greenness, and yellowness/blueness, respectively. In particular, CIELAB performs a nonlinear transformation on  $X$ ,  $Y$ , and  $Z$  aiming to linearize the perceptibility of color differences for a standard human observer under a given illuminant (usually chosen as daylight D65 within museums) [13]. This results in a perceptually uniform color space where the Euclidean distance is well correlated with the perceived color differences. In practice, this property is only fulfilled approximately, and so we usually use the term pseudo-uniform for CIELAB. Finally, we remark that any color transformation takes the form:

$$\kappa = \text{color} - \text{transformation} \left( \int_{\Lambda} \phi_k(\lambda) r(\lambda) d\lambda + n_k \right), \\ k = 1, \dots, N, \quad (4)$$

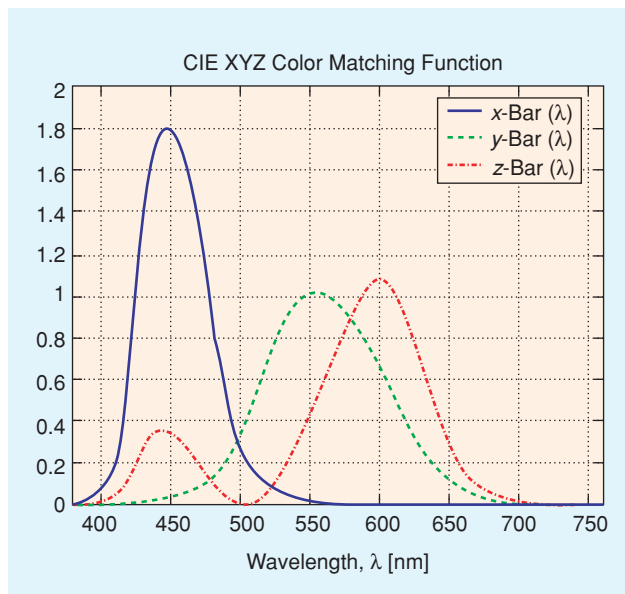


[FIG2] CIE XYZ color matching functions.

where  $\kappa$  is a 3-D vector. More details on color digital imaging can be found, for instance, in [15] or [14].

### METAMERISM

Metameric color stimuli are color stimuli with the same tristimulus values but different spectral power distributions. For color surfaces, metamers are different reflectance spectra that appear to have the same color (i.e., same tristimulus values) to the observer under a given illuminant, but may look different under other light sources. The elimination of the metamerism phenomena is a fundamental reason for the use of multispectral rather than trichromatic RGB imaging when the highest-fidelity color reproduction is required. This concept is easy to define mathematically from the description already presented. Let us call  $L$  the diagonal matrix containing  $N$  samples of the spectral radiance of the illuminant in (1) and  $A$  the  $N \times 3$  matrix containing in its successive rows the vectors  $L\bar{x}$ ,  $L\bar{y}$ , and  $L\bar{z}$ , where  $\bar{x} = [\bar{x}(\lambda_1) \bar{x}(\lambda_2) \cdots \bar{x}(\lambda_K)]^t$ ,  $\bar{y} = [\bar{y}(\lambda_1) \bar{y}(\lambda_2) \cdots \bar{y}(\lambda_K)]^t$ , and  $\bar{z} = [\bar{z}(\lambda_1) \bar{z}(\lambda_2) \cdots \bar{z}(\lambda_K)]^t$ . Then the visual tristimulus values are  $[XYZ] = A r$ , where  $r = [r(\lambda_1) r(\lambda_2) \cdots r(\lambda_K)]^t$ . Thus, two different spectral reflectances  $r_1$  and  $r_2$  are metamers if  $A r_1 = A r_2$ . Therefore, the projection  $P_A = A^T(AA^T)^{-1}A$  generates the so-called human visual illuminant subspace (HVISS) and  $P_A r$  corresponds to the definition of the fundamental metamer [16]. This concept mathematically represents the inability of the human visual system to distinguish certain spectral differences. [Please note that most of the metamerism bibliography present these formulae transposed, which is equivalent; this section is presented this way to be consistent with the rest of the document, especially (7) and (8).] Color imaging systems based on sensors with only three color filters also clearly exhibit metamerism. First, a metameric reproduction is always illuminant-dependent. Therefore, a metameric match is not sufficient if the reproduction is viewed under a variety of illuminants. Imagine the repaired finish of a green car to become a patchwork of green and brown under artificial illumination. Second, a metameric reproduction is observer-dependent. The reproduced color and the original color only match as long as the standard observer is considered. A human observer, however, usually departs slightly from the standard observer, causing a mismatch between the original and the reproduced color.

The definition of metamerism can be extended for a multi-spectral camera using their  $K$ -channel sensitivities instead of the three color matching functions  $[\bar{x} \ \bar{y} \ \bar{z}]$ . This basically means that we can calculate the spectral reflectances that will present the same responses when imaged by this camera. As a result, if we substitute the  $N \times 3$  matrix  $A$  by another  $N \times K$  matrix  $\Theta$  with  $K > 3$ , it is reasonable to expect the set of metameric reflectances with the same camera values  $\Theta r_1 = \Theta r_2$  to be progressively eliminated with increasing  $K$ . Of course, this depends on the shape of matrix  $\Theta$ , the camera projection being  $P_\Theta(r) = \Theta^T(\Theta\Theta^T)^{-1}\Theta$ . For the interested reader, the concept of the metameric black [17] may be useful in further understanding metamerism.

### CAMERA SENSITIVITY

From a signal processing point of view, the filters of a multi-spectral camera can be conceived as sampling functions, the other elements of  $\phi$  being understood as a perturbation. If we regard integral equation (1) as a sampling process, the kernel  $\phi$  would be a sampling operator (typically made from delta Diracs) and the spectral reflectance  $r(\lambda)$  would be the signal to be sampled. However, the filters are not the only elements composing  $\phi$ , nor are they Dirac functions. In Figure 3(a), we simulate the effect of ten Gaussian filters on a physical spectral reflectance. These filters are equi-distributed on the visual spectrum. We see that the output approximates the original signal. This is because 1) only the filters are taken into account in this simulation and 2) the filters are narrow-band and therefore “close” to a delta Dirac function. In Figure 3(b), we add to the simulation the illuminant radiance of a halogen lamp and the sensitivity curve of a real charge-coupled device (CCD) sensor. We now observe that the obtained responses no longer approximate the spectral reflectance. However, it could be argued that the only elements that vary in  $\phi$  are the filter transmittances and the illuminant, the sensor sensitivity remaining constant. By measuring or estimating these two spectral functions, we are able to find a linear operator that removes this “perturbation” from the sampling process. Such an approach is possible in practice and it is usual part of a spectrometric calibration.

The precise sampling of the spectral reflectance using narrow-band filters is, in effect, to create a spectrophotometer. This works best for camera configurations with a large number of narrow-band filters [12], [18]. For such cameras, an interpolation of the calibrated sensor responses is sufficient to reconstruct the original reflectance curve. Care should be taken as real filters are normally not Gaussian shaped. Moreover, when a filter is not narrow, positioning the camera responses in the spectral domain cannot be done accurately. In any case, the sampling approach is a conceptually interesting way of conceiving the camera acquisition process that gives insight into its nature. When filters are few and their shapes are neither narrow nor similar, the camera can still be used as an image spectrometer but requires an intermediate reconstruction step (see the “Spectral Reflectance” section).

### FILTER DESIGN OR SELECTION

As we have seen, filters play a very important role as “samplers” of the original spectral reflectance; consequently, their shape is a central aspect of any camera design. Also their number presents important implications, but it is not clear whether, beyond a certain number, adding more filters leads to better color quality [19]. In any case, one of the first questions that arises when designing filters is: “What are we designing the filters for?” An obvious answer to this question is “to obtain better color rendering,” which mathematically translates to minimizing color differences between vector  $\kappa$  obtained from (4) and a perfect color or color reference  $\kappa_R$ :  $\min_{\kappa} \|\kappa - \kappa_R\|$ ; see, for instance, [7]. However, in the usual case where a CIELAB color transformation is used, this

leads to a nonlinear optimization problem. Some authors such as [20] use statistical optimization to select filters from a set of available ones. In any case, whether filters are to be selected or their transmittances designed, the development of mathematical criteria for assessing filter quality is a fundamental step towards a good design. The first remarkable effort in this direction was presented by Neugebauer [42] who proposed the so-called  $q$  factor for filter optimization. This criterion

is defined as  $q(\mathbf{m}) = \|P_A \mathbf{m}\|^2 / \|\mathbf{m}\|^2$ , where  $\mathbf{m}$  represents the sampled spectral transmittance of a filter. This criterion is presented here for its pedagogical and historical importance; please note the use of the projection  $P_A \mathbf{m}$  and, consequently, the close relationship of this criterion and metamerism. In fact, the  $q$  factor is a measure of the quality of a single recording filter with negligible measurement noise and is based on the fractional energy contained in the HVISS. In any case, the

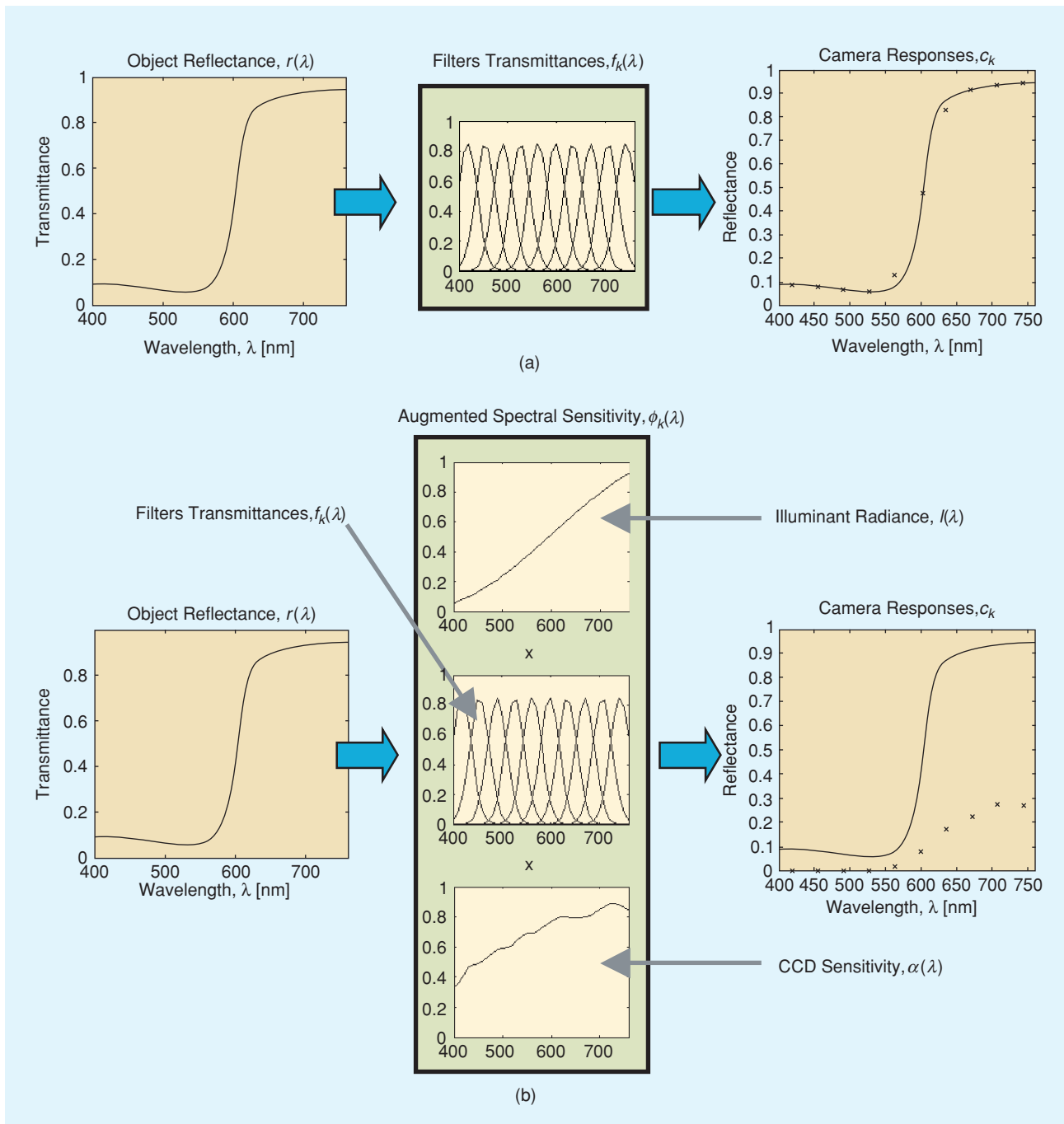


**[FIG3]** The filters as sampling functions of the spectral reflectance curves. (a) Simulation of camera acquisition using exclusively ten Gaussian filters. The crosses (camera responses) on the right panel approximate the object spectral reflectance that is superposed for reference as a continuous line. (b) Simulation of camera acquisition using a halogen lamp, ten Gaussian filters, and the sensitivity curve of a real CCD. The crosses (camera responses) on the right channels do not approximate the object spectral reflectance as in (a).

$q$  factor presents several important problems. First of all, it is not a measure for a set of filters and it is not valid for more than three filters. In the case of using three filters, they must be linearly independent. The  $q$  factor presents too many constraints to be used effectively as a design criterion but presents a basic approach for linear optimization. In that sense, Vrhel and Trussel [21] designed optimal filters using (3) which minimized in CIE-XYZ space the errors in predicting the colors of 343 patches from a color copier under several different illuminants in the presence of noise. In addition, a measure of goodness as a criterion for the selection of a set of color-scanning filters was introduced [22]. It was also shown that the color filter design problem could be simplified with the notion of an inner product [23]. In [24], the authors also introduced figures of merit for filter design, which are in better agreement with the perceptual error. The unified measure of goodness is also presented by [25], which simultaneously considers the imaging noise and its propagation, colorimetric reproduction accuracy, and multi-illuminant color correction. Recently, [26] has developed a criterion for colorimetric accuracy and has compared it via simulation when using three or more Gaussian filters. The authors of [27] have also presented insight into filter design for multispectral systems.

### LIGHTING SYSTEM

The spectral radiance of the illuminant,  $I(\lambda)$ , in (1) has always been one of the main problems in photography. Indeed, camera responses and their associated color values are highly dependent on lighting conditions. This is the reason why systems for the accurate acquisition of paintings always contain a dedicated lighting system, which is controlled in three aspects:

- 1) The temporal stability should be assured such that  $I(\lambda)$  does not depend on time.
- 2) The spectral radiance should be measured. Different spectral distributions of radiant energy induce different camera channel sensitivities; this consequently varies the acquisition parameters of the camera.
- 3) The spatial distribution of the illuminant is, in general, not homogeneous and should be characterized.

These three preceding points will be illustrated in the "Example Using the *Mona Lisa*" section by the use of the CRISATEL system.

### ACQUISITION NOISE AND CAMERA CALIBRATION

The sensor and its associated electronics are usually responsible for the main noise sources present in multispectral imaging. It is often informally said that the enemy of image quality is noise. The process of dealing with noise appears at several levels in a multispectral system. In order to better understand how to deal with it, we should know its origin, characterize it, and know how we can use this information to optimize image quality. In this section, we address these two first subjects. How to optimize image quality will then be illustrated by means of the *Mona Lisa* capture.

### UNDERSTANDING NOISE SOURCES

The noise is present in the spectral, temporal, and spatial dimensions of the image signal. We do not deal with temporal noise here because imaging of art paintings does not imply temporal recording. Concerning the spectral distribution of noise, current image sensors have a sensitivity that is not homogeneous across the spectral range.

Concerning spatial noise, the noise sources normally taken into account in the multispectral community, [7] and [28], are dark current  $N_{DC}$ , read-out noise  $N_{RO}$ , and shot noise  $N_S$ . Dark current  $N_{DC}$  is the result of imperfections or impurities in the depleted bulk silicon or at the silicon/silicon dioxide interface. The output amplifier has a resistance that causes thermal noise  $N_{RO}$ . Finally, shot noise  $N_S$  is the noise associated with the random arrival of photons at the detector. Other noise sources are normally ignored, meaning that the noise term in (1) is decomposed as follows:  $n_k = N_{DC} + N_{RO} + N_S$ . Now, based on [29], a noisy camera response can be expressed as

$$C(\tau, k) = \text{quantization}(M(\tau, k) I(\tau, k) + N_{DC}(\tau, k) + N_{RO}(k) + N_S(\tau, k)), \quad (5)$$

where  $I(\tau, k)$  represents the integral in (1) in the absence of noise; thus  $I(\tau, k) = \int_{\Lambda} I(\lambda) r(\lambda) f_k(\lambda) \alpha(\lambda) d\lambda$ . Note that spatial index  $\tau$  for the pixel position has been introduced. The introduction of a spatial index also implies the introduction of the variability map  $M(\tau, k)$ , which represents the combined variation of the lighting irradiance and the sensor sensitivity between pixels. The index  $k$  also appears in all elements of (5), indicating that noise analysis is performed independently channel by channel. Finally, the *quantization*( $\cdot$ ) operator in (5) represents the analog-to-digital (A/D) conversion performed before stocking the signal in digital form. This conversion introduces the so-called quantization error, a theoretically predictable noise.

### CHARACTERIZING NOISE

Once a model of noise is defined, its parameters should be estimated. This noise characterization implies experimental analysis where a set of images are acquired to estimate the statistics of the noise distributions defined in (5) and the variability map  $M$ .

The first step in characterizing noise is to take a series of dark images; for this, camera lenses are typically obturated by use of a cap. This is performed because it is known that dark current noise has a positive mean and fluctuates around it, while read-out noise and shot noise have zero mean. When taking dark images, we have simply  $I(\tau, k) = 0$ , and (5) becomes  $C(\tau, k) = N_{DC}(\tau, k) + N_{RO}(k) + N_S(\tau, k)$ . Acquiring a set of dark images allows the direct estimation of  $\mu_{DC}$  the positive mean of dark current noise, by simply averaging the measurements. If we define  $N_{DC} = \mu_{DC} + n_{DC}$ , then the noise terms can be decomposed as

$$n_k = \mu_{DC} + N_C + N_S, \quad (6)$$

where  $N_C = n_{DC} + N_{RO}$ . This new way of regarding noise is useful for its experimental characterization. It is now composed of: 1) one offset corresponding to  $\mu_{DC}$ , 2) a zero-mean signal-independent  $N_C$ , and 3) a zero-mean signal-dependent noise  $N_S$  corresponding to the shot noise. The variance of the global noise,  $\sigma_n^2$ , can be expressed as the sum of the variances of  $N_C$  and  $N_S$  because the occurrence of each one of these noises is independent of the other:  $\sigma_n^2 = \sigma_C^2 + \sigma_S^2$ , where  $\sigma_C^2$  and  $\sigma_S^2$  represent the variances of signal-independent and signal-dependent noises, respectively. Using a set of dark-current images, we can directly estimate the signal-independent noise  $\sigma_C^2$ . The interested reader will find mathematical details dealing with signal-dependent noise in [29].

### SPECTRAL REFLECTANCE

Before using the spectral reflectance for high-fidelity color reproduction or other uses, we should note that this property of the materials could be estimated for each pixel of the multi-spectral image. To understand how this estimation is performed, we first discretize integral (1). By uniformly sampling the spectra at  $N$  equal-wavelength intervals, we can rewrite (1) as a scalar product in matrix notation:

$$c_k = \phi_k^t r + n_k, \quad (7)$$

where  $r = [r(\lambda_1) \ r(\lambda_2) \ \dots \ r(\lambda_N)]^t$  and  $\phi_k = [\phi_k(\lambda_1) \ \phi_k(\lambda_2) \ \dots \ \phi_k(\lambda_N)]^t$  are vectors containing the sampled

spectral reflectance function and the sampled augmented spectral sensitivity of the  $k$ th channel of the acquisition system, respectively. The vector  $c_K = [c_1 c_2 \dots c_K]^t$  representing the responses of all  $K$  channels may then be described using matrix notation as

$$c_K = \Theta r + n, \quad (8)$$

where  $n = [n_1 n_2 \dots n_K]^t$  and  $\Theta$  is the  $K$ -line,  $N$ -column matrix defined as  $\Theta = [\phi_k(\lambda_n)]$ , where  $\phi_k(\lambda_n)$  is the augmented spectral sensitivity of the  $k$ th channel at the  $n$ th sampled wavelength.

The first approach to spectral reconstruction is to inverse matrix  $\Theta$  and find a reconstruction operator in the form of  $r = \text{inv}(\Theta)c_K$ . This direct inversion implies that matrix  $\Theta$  is known, which means that the CCD sensitivity and filter transmittances have been measured (i.e., [7], [30], or [31]). This typically requires a monochromator and a radiometer for measuring the CCD sensitivity and a spectrometer for measuring the spectral transmittances of the filters. We remark that matrix  $\Theta$  is, in general, not a square matrix. Typically, the spectral reflectance is sampled at 10-nm intervals giving around  $N = 40$  samples. The CRISATEL system has ten visible-color channels, and thus matrix  $\Theta$  has dimensions  $10 \times 40$ . Consequently, the system itself is underdetermined and by definition ill-posed in the sense of Hadamard [32]. As already mentioned, the noise described earlier affects the input of the

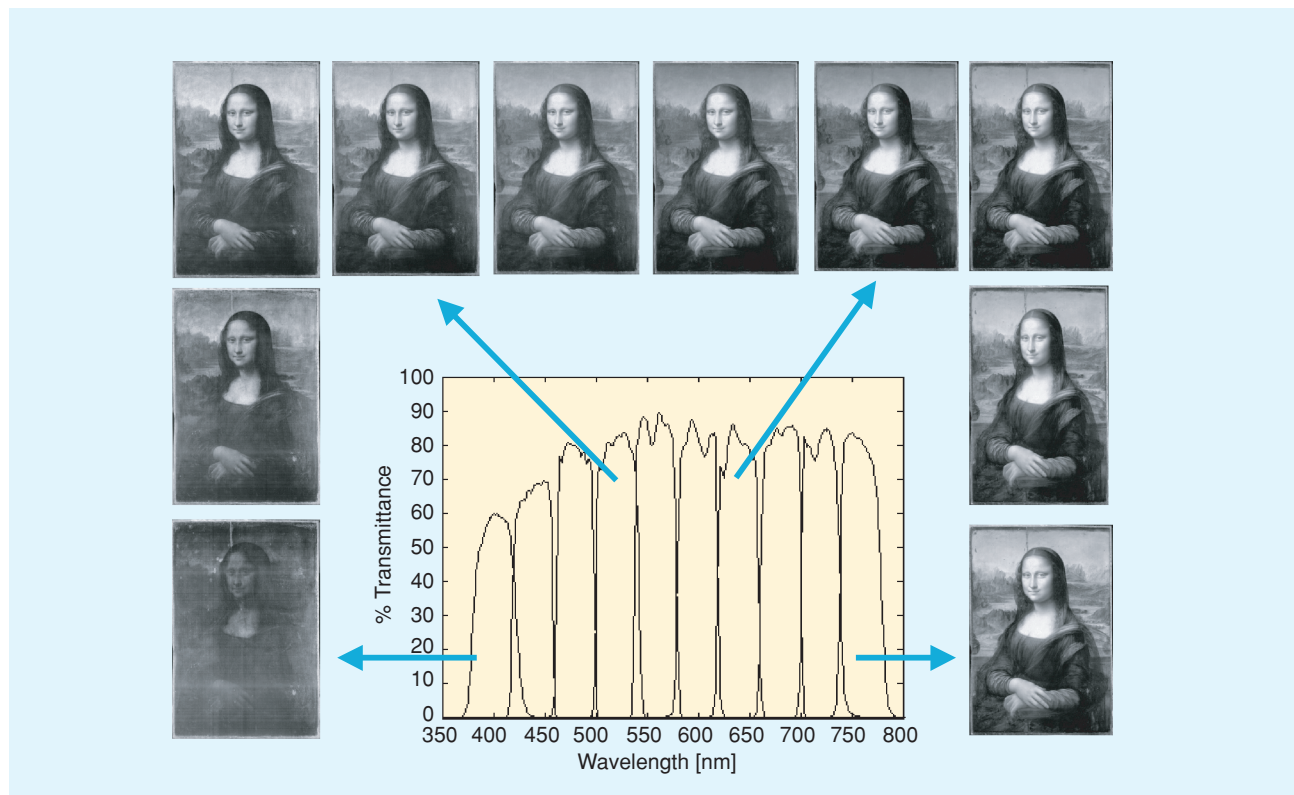


[FIG4] Transmittances of the ten visible filters measured with a Hitachi spectrophotometer. The resulting image of the *Mona Lisa* is shown for each filter. (*Mona Lisa* courtesy of the Centre de Recherche et de Restauration des Musées de France.)

reconstruction operator. This is often taken into account in the inversion of matrix  $\Theta$ . However, the inversion of matrix  $\Theta$  is not the only way of finding a reconstruction operator. Indirect reconstruction is possible when the spectral reflectance curves of a set of  $P$  color patches are known, and a multispectral camera acquires an image of these patches (i.e., [28] or [33]). From this data, a set of corresponding pairs  $(c_p, r_p)$ , for  $p = 1, \dots, P$ , is obtained, where  $c_p$  is a vector of dimension  $K$  containing the camera responses and  $r_p$  is a vector of dimension  $N$  representing the spectral reflectance of the  $p$ th patch. Corresponding pairs  $(c_p, r_p)$  are easy to obtain and professional calibrated color charts such as the Gretag Macbeth DC are sold with the measurements of the spectral reflectances of their patches. In addition, if a spectrophotometer is available, performing the measure is a fairly simple experiment. Obtaining the camera responses from the known spectral curves of the color chart is just a matter of taking a multispectral image. A simple solution for an indirect reconstruction is

$$\Theta_{\text{Indirect}}^{-1} = \mathbf{R} \mathbf{C}^t (\mathbf{C} \mathbf{C}^t)^{-1}, \quad (9)$$

where  $\mathbf{R}$  is a  $N \times P$  matrix with columns containing all the  $r_p$ s and  $\mathbf{C}$  is a  $K \times P$  matrix with columns containing their corresponding  $c_p$ s. Finally, when the camera is perfectly calibrated and numerous narrow-band filters are used, the reconstruction (as already stated in the “Camera Sensitivity” section) can be performed by interpolation of the corrected camera responses. We will not give details of the mathematical methods for spectral reflectance reconstruction; most of them are linear methods for solving ill-posed problems. For a more detailed description of these methods, please refer to [34].

### EXAMPLE USING THE MONA LISA

#### CRISATEL FILTERS

The CRISATEL camera used for the digital capture of the *Mona Lisa* (Musée du Louvre, Paris, France) uses ten equi-spaced 40-nm band-pass interferential filters in the visible domain (350–800 nm) and three wider filters, 100-nm band-pass, in the near infrared. The spectral transmittances of the ten filters in the visible domain along with the corresponding images of the *Mona Lisa* scanned with them are shown in Figure 4. Another set of filters with the same transmittances was also mounted on the VASARI camera at the National Gallery of London [35]. The 40-nm filters in the visible domain allow us to use the camera as an image spectrometer and determine the colorimetry from the spectral reflectance. Another key feature of the CRISATEL camera is its extremely high spatial resolution.

The camera delivers up to  $20,000 \times 12,000$ , 12-b data samples for each of the 13 filters, resulting in a very high resolution for both our spectral and reconstructed colorimetric images.

The transmittances of the three infrared channels are shown in Figure 5(c). As many pigments are invisible in the infrared, they are additionally

useful to visualize underdrawings, which are preparatory drawings made on a painting surface before the paint itself is applied. The underdrawings are fundamental in the study of pentimenti: an alteration in a painting evidenced by traces of previous work, showing that the artist has changed his mind as to the composition during the process of painting. The underdrawings are usually hidden by covering pigment layers and, therefore, invisible to the observer in visible light. Normally, infrared reflectograms [36] are used to study pentimenti. They are obtained with infrared sensors sensitive from 1,000 to 2,200 nm. This range is often called the fingerprint region. The CRISATEL projects decided, therefore, to use the available sensitivity of the CCD in the near infrared to obtain three infrared reflectogram channels. Figure 5(b) shows an image taken by the first infrared channel used on the *Mona*

**DIGITAL IMAGE CAPTURE TO FAITHFULLY RECORD FINE ART PAINTINGS IS A FUNDAMENTAL TASK IN A CULTURAL HERITAGE DOMAIN.**



(a) (b)

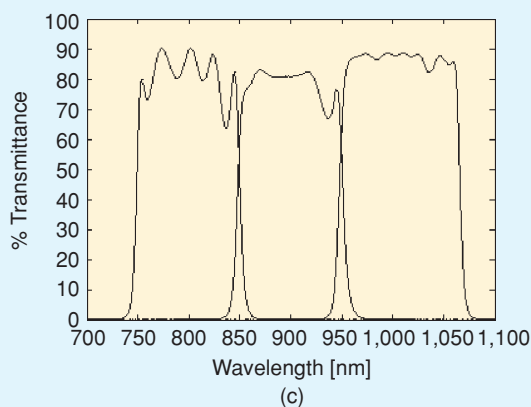


**[FIG5] Detail of the hands of the *Mona Lisa*: (a) color projection from the reconstructed spectral reflectance curves, (b) a near infra-red band, and (c) transmittance of the three infra-red filters measured with a Monolight spectrophotometer. (*Mona Lisa* courtesy of the Centre de Recherche et de Restauration des Musées de France.)**

*Lisa* and used to study pentimenti. In Figure 5(a), we can compare this image with a color rendering. Indeed, we see that under the hands of the *Mona Lisa* there is an older contour of the fingers in a different position relative to the hand.

### LIGHTING SYSTEM

In the scan of the *Mona Lisa*, hydrargyrum quartz iodide (HQI) lamps were mounted in two motorized elliptical projectors. These projectors scan the painting with a narrow band of strong light in synchronization with the motion of the linear CCD array inside the camera. Stabilized electrical systems and fully warmed-up bulbs were used in this capture. Moreover, measurements of the lighting were made to better control and stabilize the output of the bulbs.

To illustrate the significant impact of the illuminant system on the final images, we experimentally measured the relative sensitivity of the channels of the CRISATEL acquisition system for a halogen filament and an HQI lamp. The results are shown in Figure 6. Halogen filaments are presented only as an example. Their use was avoided as they produced too much heat which could have damaged the painting surface. Note how each illuminant induces strongly

different channel sensitivities. Note also the difference of sensitivity found in the infrared channels. This is due to the broader band of the filters combined with the decreasing sensitivity of the CCD at higher wavelengths.

Figure 7(a) shows the white homogeneous board acquired before the *Mona Lisa* itself was scanned in order to obtain a radiance map. This provides a

means to build a spatial correction map of the lighting spatial inhomogeneity that is applied in a postprocessing correction step. The contrast of this image has been enhanced to better visualize the low spatial frequency variations of the lighting in the painting area, original differences being much smaller. We show in Figure 7(b) the inhomogeneity of the pixel responses along a small portion of the CCD linear array when imaging a white board. Please note that the vertical scale of this graph has been zoomed to view the variations caused by noise. The ratio for an individual pixel between its response and the corresponding low-pass-filtered value (red curve) determines the gain factor correction to apply at this pixel. The CRISATEL camera has a built-in system to automatically interpose a diffuser on the optical path, which is used to acquire homogeneous-signal

FOR THE DIGITAL CAPTURE OF FINE ART PAINTINGS, THE NUMBER OF K FILTERS RANGES FROM K=7 TO RECENT K=32, DEPENDING ON THE SIZE OF THE FILTER BAND.

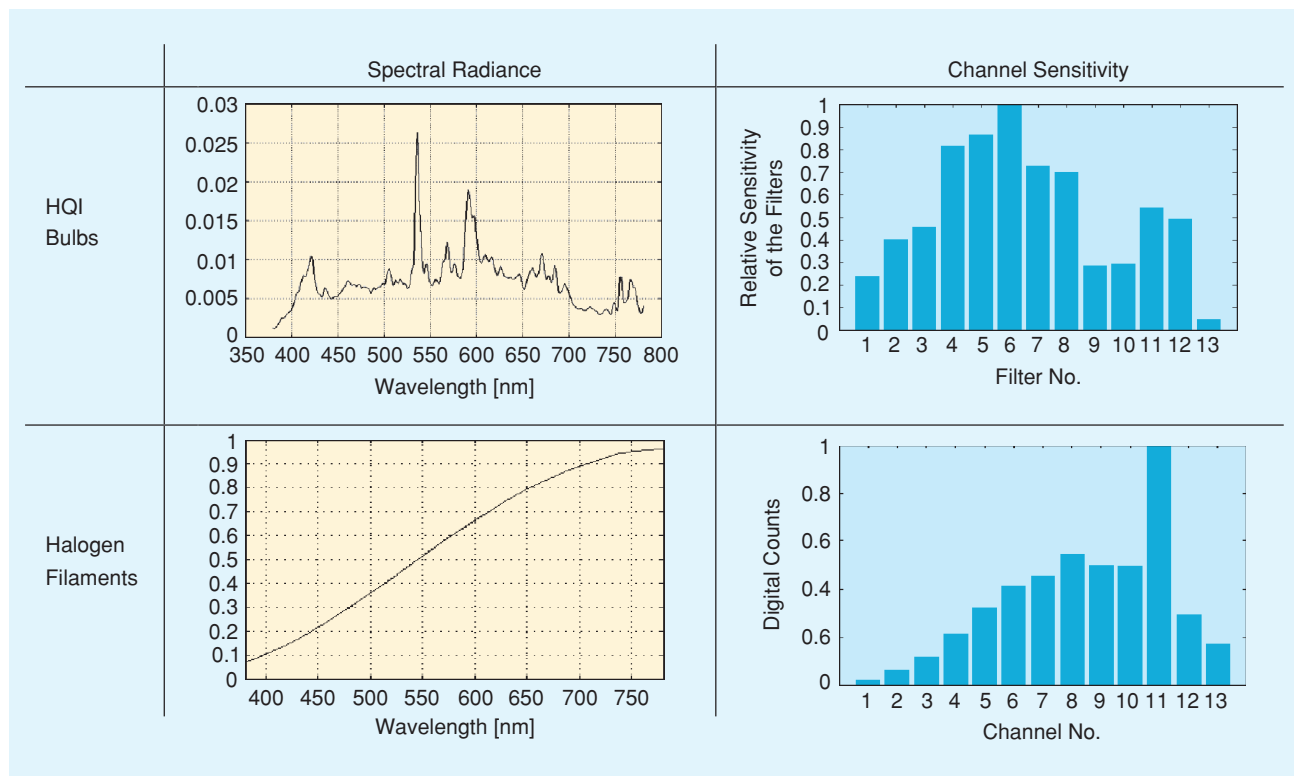


**[FIG6]** Effect of the illuminant on the channel sensitivity. The left column shows the measured spectral distribution of the radiant energy of the HQI bulbs and the halogen filaments used in the CRISATEL lighting system. The right column shows the relative augmented channel sensitivity responses of the CRISATEL camera. Channels 1–10 correspond to the ten filters in the visible spectral range, and channels 11–13 to the three IR filters.

images with only very low spatial frequencies [not used in Figure 7(b)].

**NOISE**

The spectral sensitivity curve of the Thomson CCD used in the CRISATEL camera can be seen in Figure 3(b). As we can see, the CCD is less sensitive at low wavelengths (blue colors) and increases for red and near-infrared areas. This illustrates a typical behavior of current image sensors and means that the blue channels will require a longer exposure time with consequently

more noise corruption than red channels. This can be appreciated by comparing the *Mona Lisa* 400-nm channel image with, for example, the 600-nm channel image in Figure 4. Also concerning the CCD, we can claim that the pixel variability observed in Figure 7(b) is caused by the inhomogeneous response to light.

**USING KNOWLEDGE ABOUT NOISE**

Once the noise model in (5) has been characterized by fitting experimental data, it can be used for the three following main purposes:

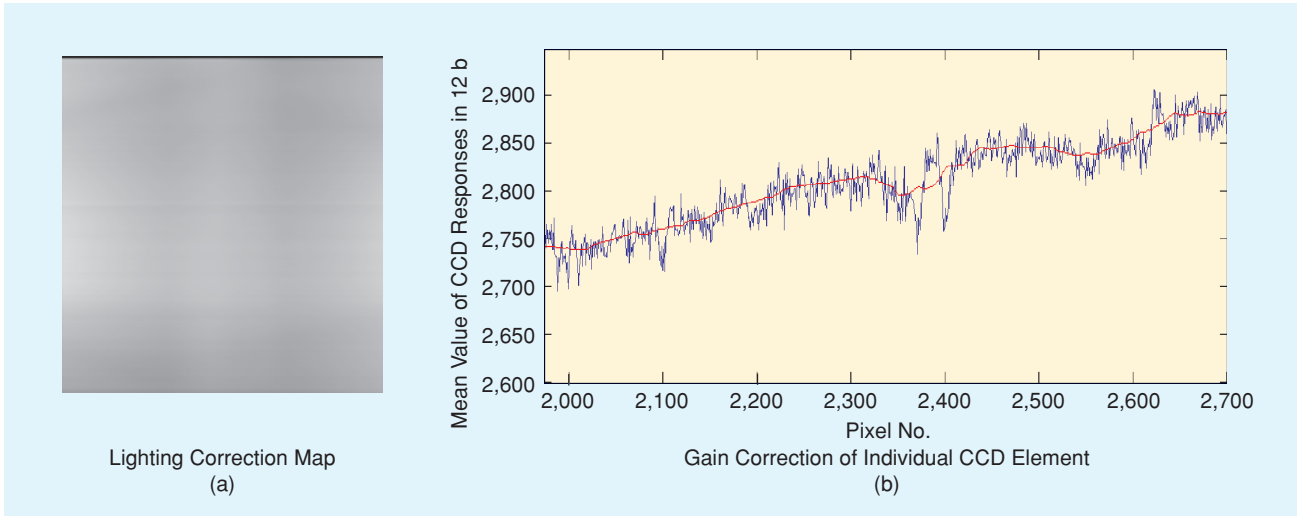


**[FIG7]** (a) Image of a white homogeneous board. This image has been contrast enhanced to visually show spatial lighting inhomogeneities and it is used to calculate the correction map used in the *Mona Lisa* scan. (b) Detail of CCD responses of the linear array when imaging a white board with a diffuser. Note the differences between a pixel and its filtered value (in red).

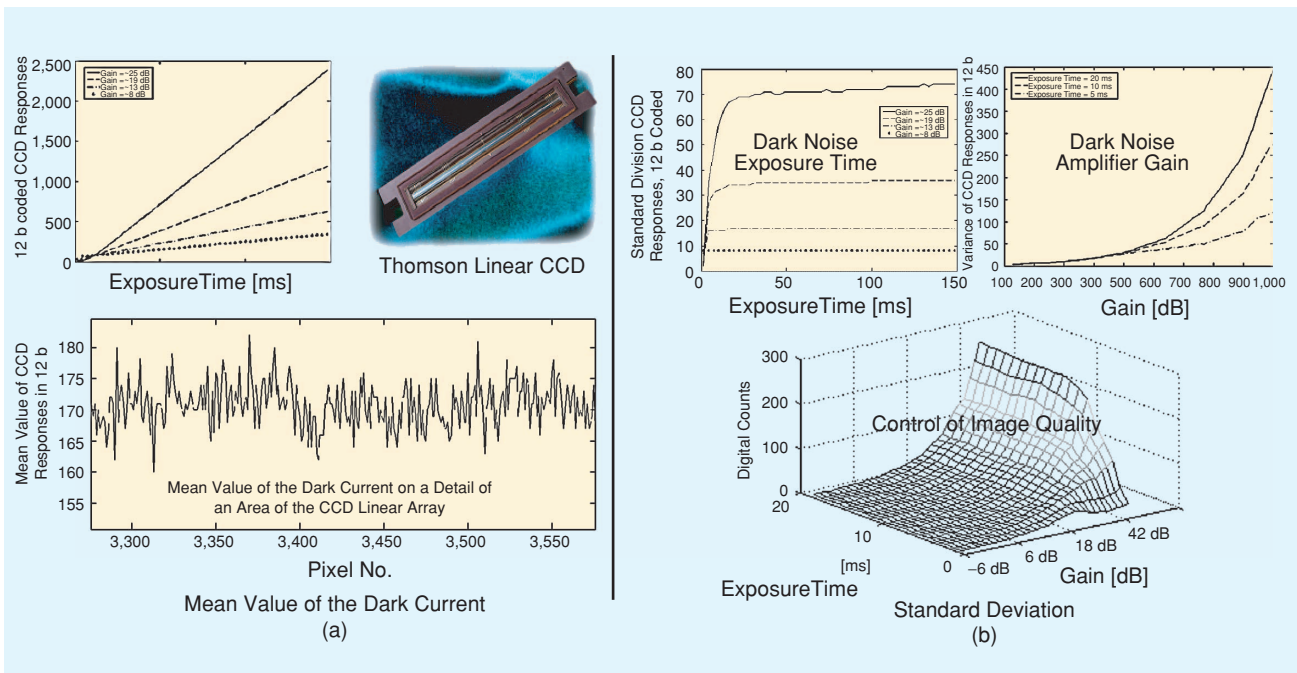


**[FIG8]** Independent-signal noise characterization for the CRISATEL CCD sensor: (a) mean value of the dark current on a detail of an area of the CCD linear array and (b) dark noise as a function of exposure time and amplifier gain.

1) *To fix the camera parameters to minimize noise.* The bottom curve shown in Figure 8(b) allows the combination of exposure time and amplifier gain to be chosen that minimizes the effect of the signal-independent noise variance,  $\sigma_C^2$ . It is important to note that fixing the camera parameters properly is extremely important for image quality. For instance, badly chosen parameters which correspond to a high  $\sigma_C^2$  are equivalent to reducing bit depth. Even if the CRISATEL camera has 12-b A/D converters, a bad decision in this step could lead it to perform as if having only 7 b.

2) *To correct the acquired images via postprocessing.* The correction system proceeds channel by channel and pixel by pixel to accomplish the following sequential operations:

**THE COLOR OF A SURFACE POINT LIT BY A GIVEN ILLUMINANT CAN BE EASILY PREDICTED WHEN THE SPECTRAL REFLECTANCE OF THE SURFACE AT THAT POINT AND THE RELATIVE SPECTRAL POWER DISTRIBUTION OF THE ILLUMINANT ARE KNOWN.**

a) *Correction of the individual behavior of the CCD pixels by using per pixel dark current offsets (subtraction of  $\mu_{DC}$  applied to the raw pixel value).* Figure 8(a) illustrates the study of  $\mu_{DC}$  for the Thomson CCD linear array used in the CRISATEL project: 1) the top-left panel shows its linear relationship with exposure time which changes in slope with the camera amplifier's gain and 2) the bottom-left panel shows a spatial map of dark current mean for a small area of the CDD.

b) *Correction of the individual behavior of the CCD pixels by using the per pixel gains (multiplicative correction applied to compensate signal-dependent noise).* To estimate  $\sigma_S^2$ , we use the built-in diffuser of the camera when imaging a homogeneous white board.

c) *Correction of the spatial inhomogeneities,  $M(\tau, k)$ .* This is also estimated from a diffuse image of a homogeneous white board.

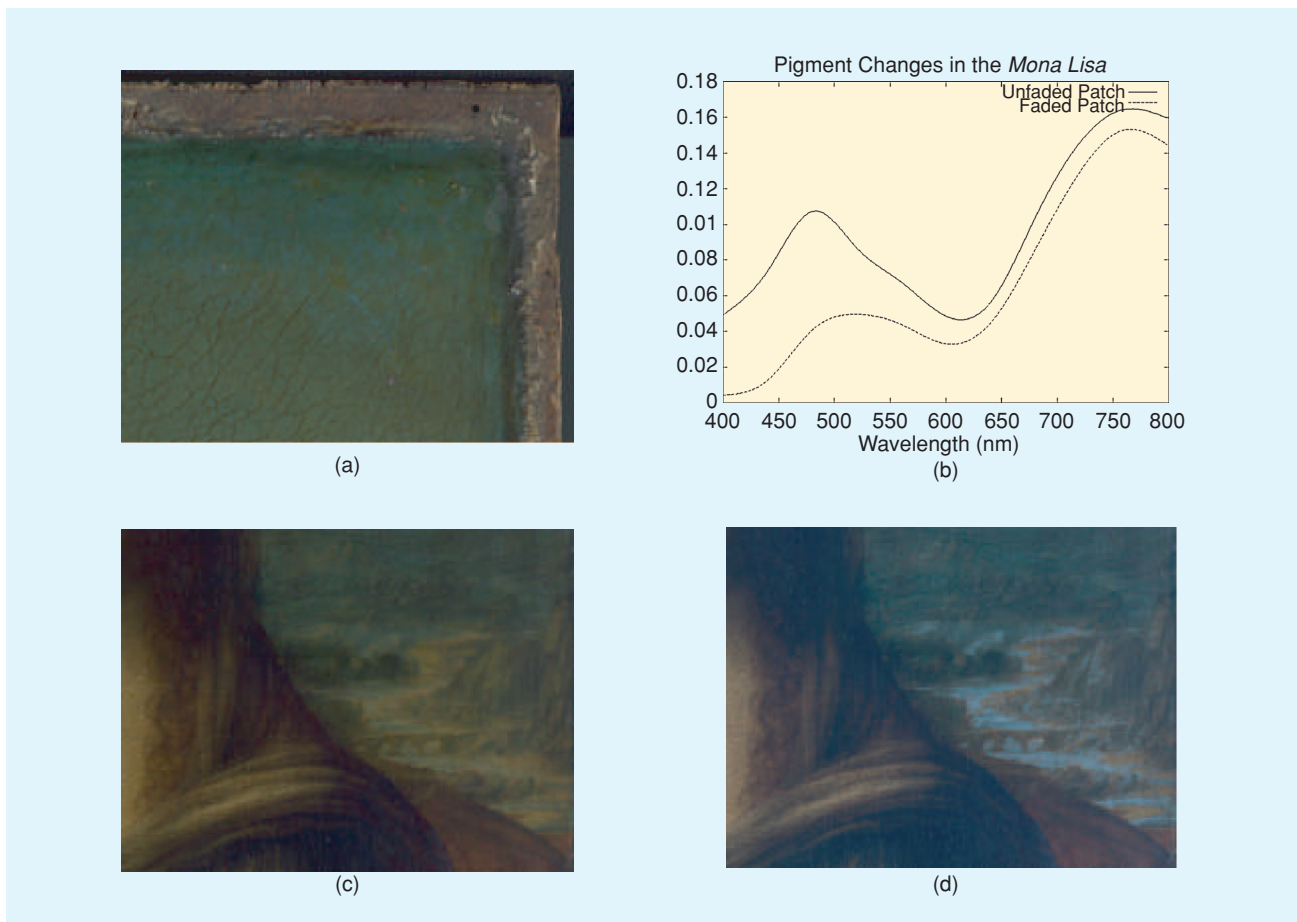


**[FIG9]** Unfading the *Mona Lisa* (detail) by use of a nondegraded reference pigment found under the frame: (a) unfaded pigments found under the frame, (b) spectral reflectances of faded and unfaded patches, (c) faded pigment in the background (original colors), and (d) pigment unfading applied to the painting (predicted original colors). (*Mona Lisa* courtesy of the Centre de Recherche et de Restauration des Musées de France.)

3) To stabilize the resolution of inverse problems. Knowledge about the noise can also be used, for instance, to stabilize the estimation of filter transmittances or for spectral reflectance reconstruction [7].

IN THE SCAN OF THE MONA LISA, HQI LAMPS WERE MOUNTED IN TWO MOTORIZED ELLIPTICAL PROJECTORS.

### SPECTRAL REFLECTANCE USES IN FINE ART PAINTING

The determination of a spectral reflectance per pixel for a painting opens up a wide range of potential applications. From (1) we see that such an image is independent of the lighting conditions and the acquisition system. This is the main reason why high-fidelity color reproduction is possible. The CRISATEL system intrinsically deals with and controls the problem of metamerism, producing accurate rendering under any combination of observer and illuminant [37]. However, this requires an accurate reconstruction of the spectral reflectance. This accuracy was a key requirement when building the CRISATEL system and the results from using various reflectance reconstruction methods using the camera can be found in [38]. In addition, a method using mixture density networks was specifically developed for the system, which proved to be the most accurate of the methods tested [39]. When dealing with works of art, the spectral reflectance also has other uses. For instance, it is possible to characterize the palette of the artist's pigments or even to identify the pigments by comparison of their spectral reflectance curves with a reference. Furthermore, models of pigment aging and devarnishing can be applied to obtain estimations of the original painting appearance at the moment it was painted. We will briefly show in the following example some results of the virtual devarnishing of the *Mona Lisa*. We will not consider other applications here; their scope and technical details do not fit the limited space of this tutorial.

With the exception of catastrophic events, such as fires, floods, and physical disasters, light is the most important and insidious cause of deterioration of paintings. Exposure to light causes color changes due to photo-oxidation or photo-reduction of the painted layer. Photo-damaging is cumulative and irreversible; there is no known way of restoring colors once they have been altered by the process [40]. Although transparent UV-absorbing varnishes can be used to prevent or slow down photo-damaging in oil paintings, they also become photo-oxidized and turn yellow, thus requiring periodic restoration. Unfortunately, restoration is not only costly, but can also be harmful, since each time a painting is restored, there is the risk of removing some pigment along with the unwanted deteriorated varnish. Color changes can often be seen by comparing deteriorated with nondeteriorated areas, i.e., [41]. A computational method for "virtually restoring" the *Mona Lisa* colors is presented in Figure 9 based on a simple linear spectral mapping. The upper background of the *Mona Lisa* representing the sky was almost certainly blue when it was painted. Indeed, there are several patches near the corners of the painting which are normally protected by

the frame, see Figure 9(b). These patches have retained their original blue color; we call  $r_{\text{unfad}}(\lambda)$  an average representation of their spectral reflectances. Our approxima-

tion maps spectra from surrounding faded areas  $r_{\text{fad}}(\lambda)$  to those of the undamaged color patches. More extensive virtual restoration based on a more sophisticated modeling of the varnish layer and pigments themselves will be a topic of further study. Nevertheless, in this way we can attempt to simulate the state of the painting as it may have looked 500 years ago. For that,  $r_{\text{corr}}(\lambda) = r(\lambda) (r_{\text{unfad}}(\lambda) / r_{\text{fad}}(\lambda))$  is used, where  $r_{\text{corr}}(\lambda)$  stands for the corrected spectral reflectance and  $r(\lambda)$  is the reflectance estimated from the multispectral signal at one pixel of the image. In Figure 9, this transform has been applied to areas of the background which are within  $\pm 10\%$  root mean square of the spectral curve shape of the faded river. Figure 9(c) shows the *Mona Lisa* as it is today and Figure 9(d) shows an approximation of how it may have looked when freshly painted.

### CONCLUSIONS

In this article, we have presented a tutorial description of the multispectral acquisition of images from a signal processing point of view.

### ACKNOWLEDGMENTS

We extend our sincere thanks to the Département des peintures of Musée du Louvre, Paris, France, for permission to use the images.

### AUTHORS

*Alejandro Ribés* (alejandro.ribes@gmail.com) received a computer science and engineering degree (bachelor's and master's) from the University Jaume I, Castelló, Spain. He also holds a master's in image processing and computer vision from the University of Nice-Sophia Antipolis, France, and a Ph.D. in multispectral imaging applied to fine art paintings from the Ecole Nationale Supérieure des Télécommunications, Paris, France. He has been a postdoctoral fellow at the French Atomic Energy Commission, Orsay, France. He has been a research assistant at the University of Oxford, U.K., and a lecturer at the Computer Science Department of Ecole Polytechnique, Palaiseau, France. He is currently a visiting scholar at the National Yang-Ming University, Taipei, Taiwan.

*Ruven Pillay* (ruven.pillay@gmail.com) is a research scientist at the C2RMF (the National Research and Restoration Centre in the Louvre, Paris, France) working on multispectral digital imaging, colorimetry, content-based image recognition, 3-D modelization, ontologies, and the semantic Web. He has over a decade of experience in scientific research within the museum sector, having worked at the Scientific Department of the National Gallery in London before coming to the C2RMF. He has been involved in multispectral imaging

during this time having participated in both the VASARI and CRISATEL projects.

**Francis Schmitt** (francis.schmitt@enst.fr) received an engineering degree from Ecole Centrale de Lyon, France, in 1973 and a Ph.D. degree in applied physics from the University Pierre et Marie Curie, Paris, in 1979. He has been a member of Télécom Paris (Ecole Nationale Supérieure des Télécommunications) since 1973. He is currently a full professor at the Image and Signal Processing Department and head of the image processing group. His main interests are in color image analysis and synthesis, multispectral imagery, colorimetry, computer vision, 3-D modeling, and image and 3-D object indexing. He has authored or coauthored about 200 publications in these fields.

**Christian Lahanier** (christian.lahanier@free.fr) entered the national research laboratory of the museums of France in 1968 and was in charge of the physics service. He developed new nondestructive techniques of analysis of works of art. He initiated the project to create the AGLAE particle accelerator in 1987, and was responsible for the Department of Documentation and New Information Technologies at the C2RMF. He has either directed or taken part in 13 EU projects and numerous national projects.

## REFERENCES

- [1] P.H. Lewis, K. Martinez, F.S. Abas, M.F.A. Fauzi, S.C.Y. Chan, M. Addis, M.J. Boniface, P. Grimwood, A. Stevenson, C. Lahanier, and J. Stevenson, "An integrated content and metadata based retrieval system for art," *IEEE Trans. Image Processing (Special Issue on Image Processing for Cultural Heritage)*, vol. 13, no. 3, pp. 416–429, Mar. 2004.
- [2] H. Maitre, F. Schmitt, and C. Lahanier, "15 years of image processing and the fine arts," *Proc. 2001 IEEE Int. Conf. Image Processing*, Oct. 2001, vol. 1, pp. 557–561.
- [3] M. Barni, A. Pelagotti, and A. Piva, "Image processing for the analysis and conservation of paintings: opportunities and challenges," *IEEE Signal Processing Mag.*, vol. 22, no. 5, pp. 141–144, 2005.
- [4] K. Martinez, J. Cupitt, D. Saunders, and R. Pillay, "Ten years of art imaging research," *Proc. IEEE*, Jan. 2002, vol. 90, no. 1, pp. 28–41.
- [5] L. MacDonald, *Digital Heritage: Applying Digital Imaging to Cultural Heritage*. Oxford, U.K.: Butterworth-Heinemann, 2006.
- [6] F. Imai, M. Rosen, and R. Berns, "Multi-spectral imaging of Van Gogh's self-portrait at the national gallery of art Washington, D.C.," in *Proc. IS&T's 2001 PICS Conf.*, Montreal, Quebec, Canada, 2001, pp. 185–189.
- [7] H. Haneishi, T. Hasegawa, A. Hosoi, Y. Yokoyama, N. Tsumura, and Y. Miyake, "System design for accurately estimating the spectral reflectance of art paintings," *Appl. Opt.*, vol. 39, no. 35, pp. 6621–6632, 2000.
- [8] R.S. Berns, "The science of digitizing paintings for color-accurate image archives," *J. Imag. Sci. Tech.*, vol. 45, no. 4, pp. 305–325, July–Aug. 2001.
- [9] H. Brettel, J.Y. Hardeberg, and F. Schmitt, "WebCam for interactive ultispectral measurements," in *Color Imaging: Vision and Technology*, L.W. MacDonald and M.R. Luo, Eds. New York: Wiley, 2002, pp. 132–150.
- [10] J.Y. Hardeberg, F. Schmitt, and H. Brettel, "Multispectral color image capture using liquid crystal tunable filter," *Opt. Eng.*, vol. 41, pp. 2532–2548, 2002.
- [11] S. Poger and E. Angelopoulou, "Selecting components for building multispectral sensors," *IEEE CVPR Technical Sketches*, Dec. 2001.
- [12] P. Carcagni, A.D. Patria, R. Fontana, M. Greco, M. Mastroianni, M. Materazzi, E. Pampaloni, and L. Pezzati, "A scanning spectrometer for multispectral color imaging of painted surfaces," in *Proc. EVA2005*, Florence, Italy, Mar. 14–18, 2005, pp. 174–179.
- [13] G. Wyszecki and W.S. Stiles, *Color Science: Concepts and Methods, Quantitative Data and Formulae*, 2nd ed. New York: Wiley, 2000.
- [14] R.S. Berns, *Billmeyer and Saltzman's Principles of Color Technology*, 3rd ed. New York: Wiley, 2000.
- [15] G. Sharma and H.J. Trussell, "Digital color imaging," *IEEE Trans. Image Processing*, vol. 6, no. 7, pp. 901–932, Jul. 1997.
- [16] J.B. Cohen and W.E. Kappauf, "Metameric color stimuli, fundamental metamers and Wyszecki's metameric blacks," *Amer. J. Psychol.*, vol. 95, pp. 537–564, 1982.
- [17] G. Wyszecki, "Evaluation of metameric colors," *J. Opt. Soc. Amer.*, vol. 48, pp. 451–454, 1958.
- [18] G.P. Herzog and B. Hill, "Multispectral imaging and its applications in the textile industry and related fields," in *Proc. PICS03: The Digital Photography Conf.*, Rochester, NY, 2003, pp. 258–263.
- [19] D. Connah, A. Alsam, and J.Y. Hardeberg, "Multispectral imaging: How many sensors do we need?" *J. Imaging Sci. Tech.*, vol. 50, no. 1, pp. 45–52, Jan.–Feb., 2006.
- [20] J.Y. Hardeberg, "Filter selection for multispectral color image acquisition," *J. Imaging Sci. Tech.*, vol. 48, no. 2, pp. 105–110, 2004.
- [21] M.J. Vrhel and H.J. Trussell, "Optimal color filters in the presence of noise," *IEEE Trans. Image Processing*, vol. 4, no. 6, pp. 814–823, June 1995.
- [22] P. Vora and H.J. Trussell, "Mathematical methods for the design of color scanning filters," *IEEE Trans. Image Processing*, vol. 6, no. 2, pp. 312–320, Feb. 1997.
- [23] P. Vora, "Inner products and orthogonality in color recording filter design," *IEEE Trans. Image Processing*, vol. 10, no. 4, pp. 632–642, Apr. 2001.
- [24] G. Sharma and H.J. Trussell, "Figures of merit for color scanners," *IEEE Trans. Image Processing*, vol. 6, no. 7, pp. 990–1001, July 1997.
- [25] S. Quan, N. Ohta, R.S. Berns, X. Jiang, and N. Katoh, "Unified measure of goodness and optimal design of spectral sensitivity functions," *J. Imaging Sci. Tech.*, vol. 46, no. 6, pp. 485–497, 2002.
- [26] N. Shimano, "Optimization of spectral sensitivities with Gaussian distribution functions for a color image acquisition device in the presence of noise," *Opt. Eng.*, vol. 45, no. 1, p. 13201, Jan. 2006.
- [27] Ng. Du-Yong and J.P. Allebach, "A subspace matching color filter design methodology for a multispectral imaging system," *IEEE Trans. Image Processing*, vol. 15, no. 9, pp. 2631–2643, Sept. 2006.
- [28] P.D. Burns, *Analysis of Image Noise in Multitraitement Color Acquisition*, Ph.D. dissertation, Center for Imaging Science, Rochester Institute of Technology, Rochester, NY, 1997.
- [29] G.E. Healey and R. Kondepudy, "Radiometric CCD camera calibration and noise estimation," *IEEE Trans. Pattern Anal. Mach. Intell.*, vol. 16, pp. 267–276, Mar. 1994.
- [30] W.K. Pratt and C.E. Mancill, "Spectral estimation techniques for the spectral calibration of a color image scanner," *Appl. Opt.*, vol. 15, no. 1, pp. 73–75, 1976.
- [31] J.Y. Hardeberg, F. Schmitt, H. Brettel, J. Crettez, and H. Maitre, "Multispectral image acquisition and simulation of illuminant changes," in *Color Imaging: Vision and Technology*, L.W. MacDonald and M.R. Luo, Eds. New York: Wiley, 1999, pp. 145–164.
- [32] J. Hadamard, *Sur les problèmes aux dérivées partielles et leur signification physique*, Bull. University of Princeton, Princeton, NJ, 1902, pp. 49–52.
- [33] F.H. Imai, L.A. Taplin, and E.A. Day, "Comparison of the accuracy of various transformations from multi-band image to spectral reflectance," *Tech. Rep.*, Rochester Institute of Technology, Rochester, NY, 2002.
- [34] A. Ribés and F. Schmitt, "Linear inverse problems in imaging," *IEEE Signal Processing Mag.*, vol. 25, no. 4, pp. 84–99, 2008.
- [35] H. Liang, D. Saunders, and J. Cupitt, "A new multispectral imaging system for examining paintings," *J. Imaging Sci. Tech.*, vol. 49, no. 6, pp. 551–562, 2005.
- [36] J.R.J. Van Asperen de Boer, "Infrared reflectography: A method for the examination of paintings," *Appl. Opt.*, vol. 7, no. 9, pp. 1711–1714, 1968.
- [37] P. Colantoni, D. Pitzalis, R. Pillay, and G. Aitken, "GPU spectral viewer: Analysing paintings from a colorimetric perspective," in *Proc. 8th Int. Symp. Virtual Reality, Archaeology and Cultural Heritage (VAST)*, 2007, pp. 125–132.
- [38] A. Ribés, F. Schmitt, R. Pillay, and C. Lahanier, "Calibration, spectral reconstruction and illuminant simulation for CRISATEL: An art paint multispectral acquisition system," *J. Imaging Sci. Tech.*, vol. 49, no. 6, pp. 463–473, 2005.
- [39] A. Ribés and F. Schmitt, "A fully automatic method for the reconstruction of spectral reflectance curves by using mixture density networks," *Pattern Recog. Lett.*, vol. 24, no. 11, pp. 1691–1701, 2003.
- [40] T. Brill, *Light: Its Interaction with Art and Antiquities*. New York: Plenum Press, 1980.
- [41] M. Pappas and I. Pitas, "Digital color restoration of old paintings," *IEEE Trans. Image Processing*, vol. 2, pp. 291–294, Feb. 2000.
- [42] H.E.J. Neugebauer, "Quality factor for filters whose spectral transmittances are different from color mixture curves, and its application to color photography," *J. Opt. Soc. Amer.*, vol. 46, p. 821, 1956.